Supporting Material for:

Phosphorylation in the Catalytic Cleft Stabilizes and Attracts Domains of a Phosphohexomutase

Jia Xu, Yingying Lee, Lesa J. Beamer, and Steven R. Van Doren

Biochemistry Dept., 117 Schweitzer Hall, Univ. of Missouri, Columbia, MO 65211 USA

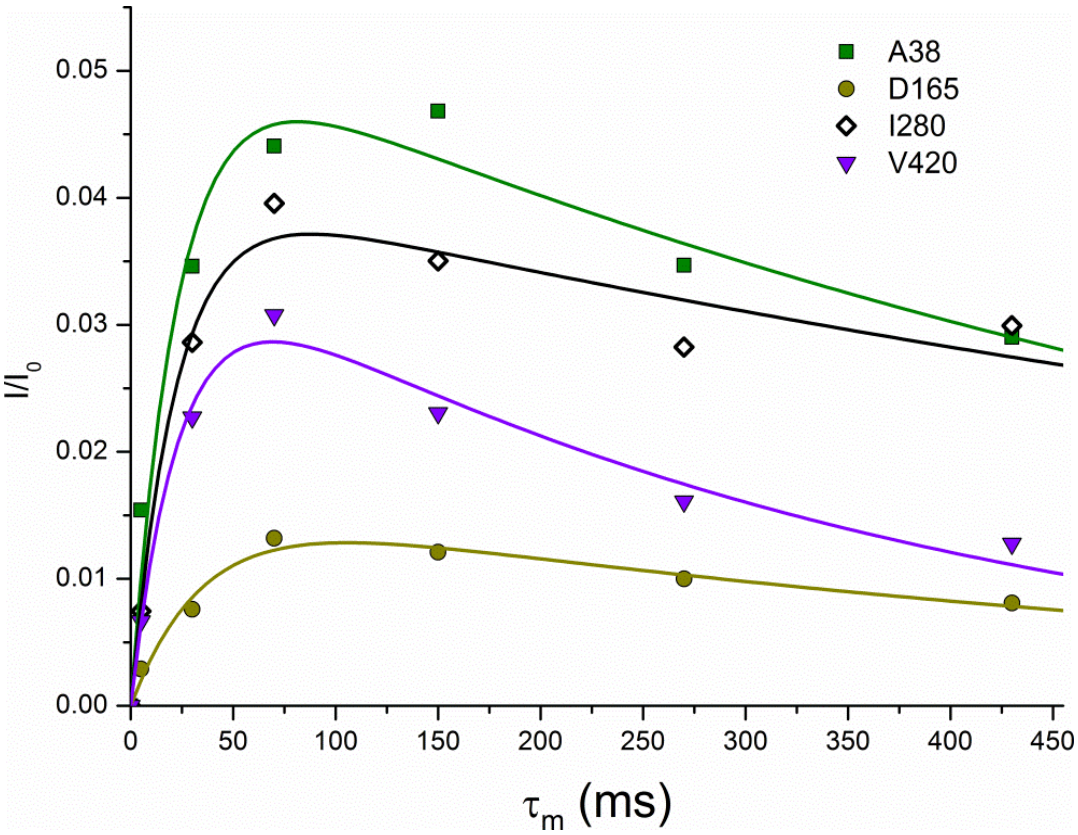

Figure S1. Examples of CLEANEX-PM time courses for the Apo-deP form of PMM/PGM. The fitted rate constants, k_{ex}, of Ala38, Asp165, Ile280, and Val420 are 2.8 ± 0.8 s^{-1}, 0.5 ± 0.1 s^{-1}, 1.9 ± 0.3 s^{-1}, and 1.1 ± 0.2 s^{-1}, respectively. These rate constants were used to simulate sub-second components of hydrogen exchange in the inset of Fig. 2D. The spin-lock during the mixing period used a radiofrequency field strength of 6.25 kHz. To maintain sample conditions consistent among the spectra during acquisition, the CLEANEX spectra were acquired in an interleaved manner and stored as a pseudo 3D spectrum. The interleaved pulse sequence and script developed to acquire and process the spectra are available as other Supplemental files.

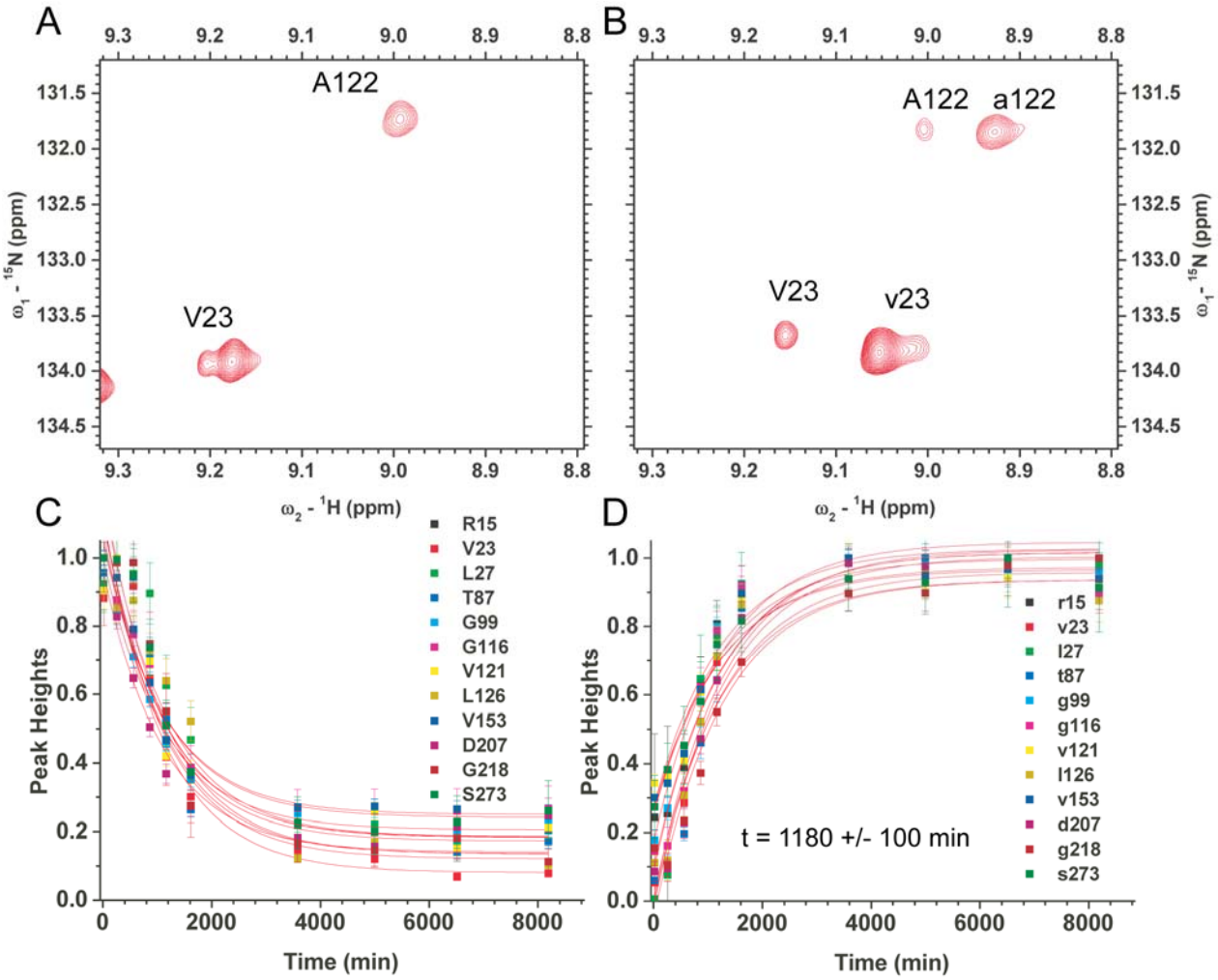

Figure S2. Kinetics of the apo-P form of PMM/PGM undergoing dephosphorylation. (A) Peaks of Val23 and Arg122 of Apo-deP 15 min after preparation are shown. (B) Peaks of the same sample after 60 h of dephosphorylation are shown. (C) The time course of the disappearance of 12 twelve normalized peaks representing the phosphorylated form is plotted. (D) The time course of the appearance of the peaks of the dephosphorylated form is plotted for the same 12 residues. These 12 used for illustration are a subset of the 43 actually used in global fits of the dephosphorylation kinetics that yielded a time constant of 1140 ± 70 min or 19.0 ± 1.1 h (where the uncertainty quoted is four-fold the fitting uncertainty).The TROSY NMR spectra were acquired at 35 °C, pH 7.5, 10 mM DTT, and 800 MHz.

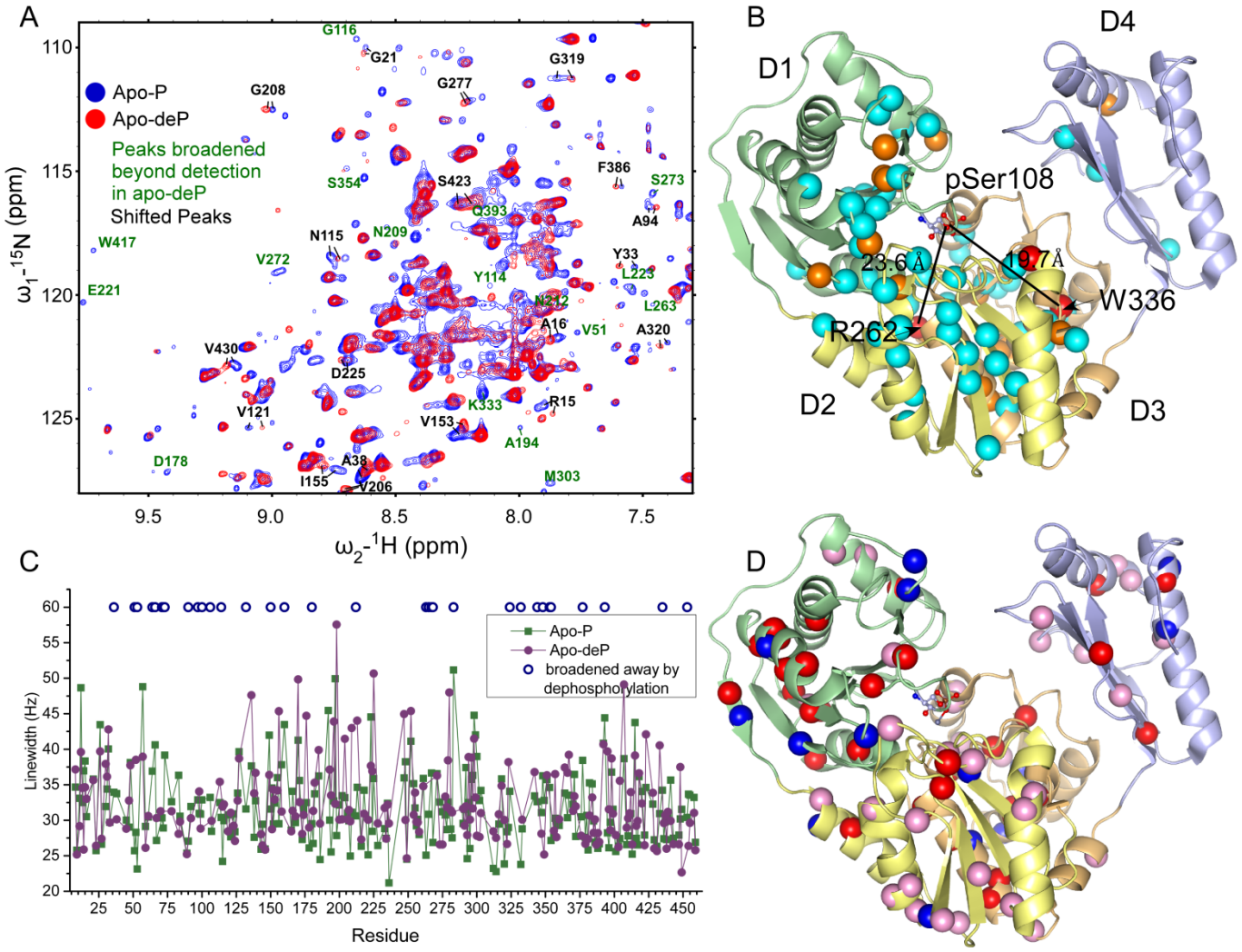

Figure S3. Effects of (de)phosphorylation on NMR spectra of PMM/PGM. (A) ^{15}N TROSY spectra of phosphorylated PMM/PGM (Apo-P; blue contours) and dephosphorylated PMM/PGM (Apo-deP; red) are superimposed. Dephosphorylation broadened beyond detection the peaks with green labels. The greater number of peaks of Apo-P reflects their being sharper and more readily detected. Conditions were 1 mM enzyme, pH 7.4, 308 K, and 800 MHz. (B) Locations of chemical shift perturbations introduced by dephosphorylation are marked on the crystal structure of Apo-P (PDB: 1K35) with red spheres for $\Delta\omega_{HN} > 0.2$ ppm, orange for $\Delta\omega_{HN} > 0.1$ ppm, and cyan for $\Delta\omega_{HN} > 0.03$ ppm, where $\Delta\omega_{HN} = ((\Delta\omega_H)^2 + (\Delta\omega_N/5)^2)^{1/2}$. The locations of Arg262 and Trp336 with the peaks most shifted by dephosphorylation are labeled along with their distances from pSer108. (C) Peaks broadened away by dephosphorylation are marked by open circles at top. The line widths plotted are each a composite of ^{1}H and ^{15}N line widths at half-height: $((\Delta\nu_{1/2,H})^2 + (\Delta\nu_{1/2,N})^2)^{1/2}$. (D) Amide peak broadenings by dephosphorylation are mapped on the structure in red where broadened away and pink where broadened > 20%, whereas blue marks amide peaks > 20% sharper in Apo-deP.

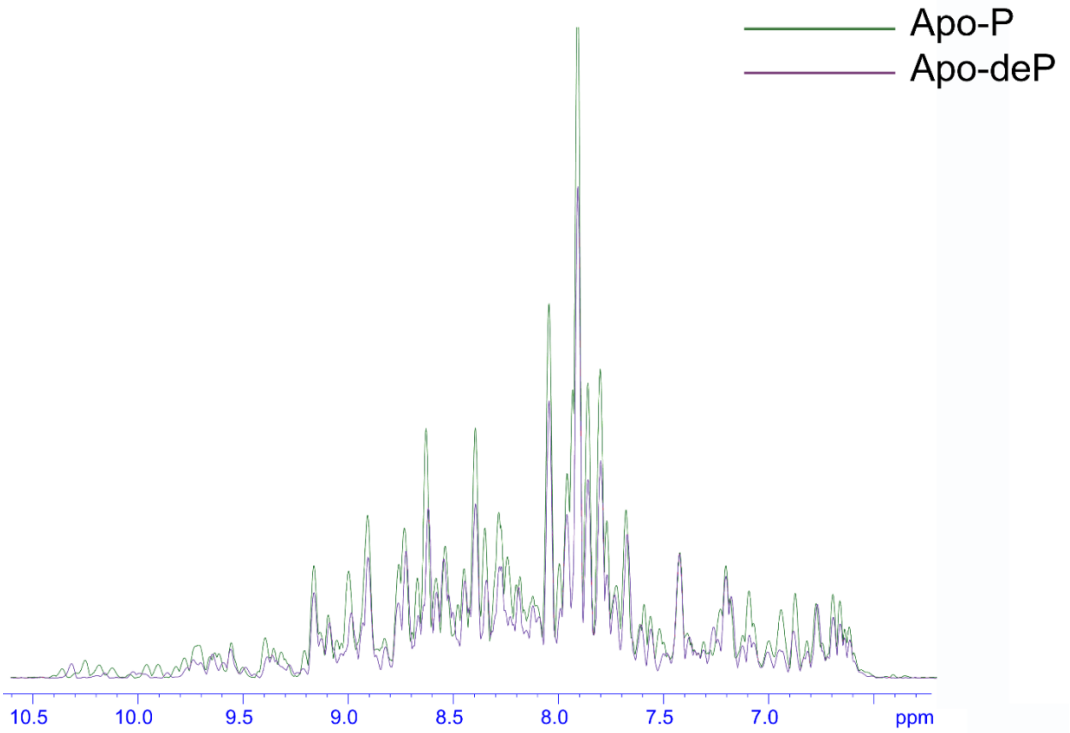

Figure S4. Skyline projections of 2D TROSY spectra of Apo-P before (green) and after more than 3 days at 35 °C where it has undergone dephosphorylation to apo-deP (purple).

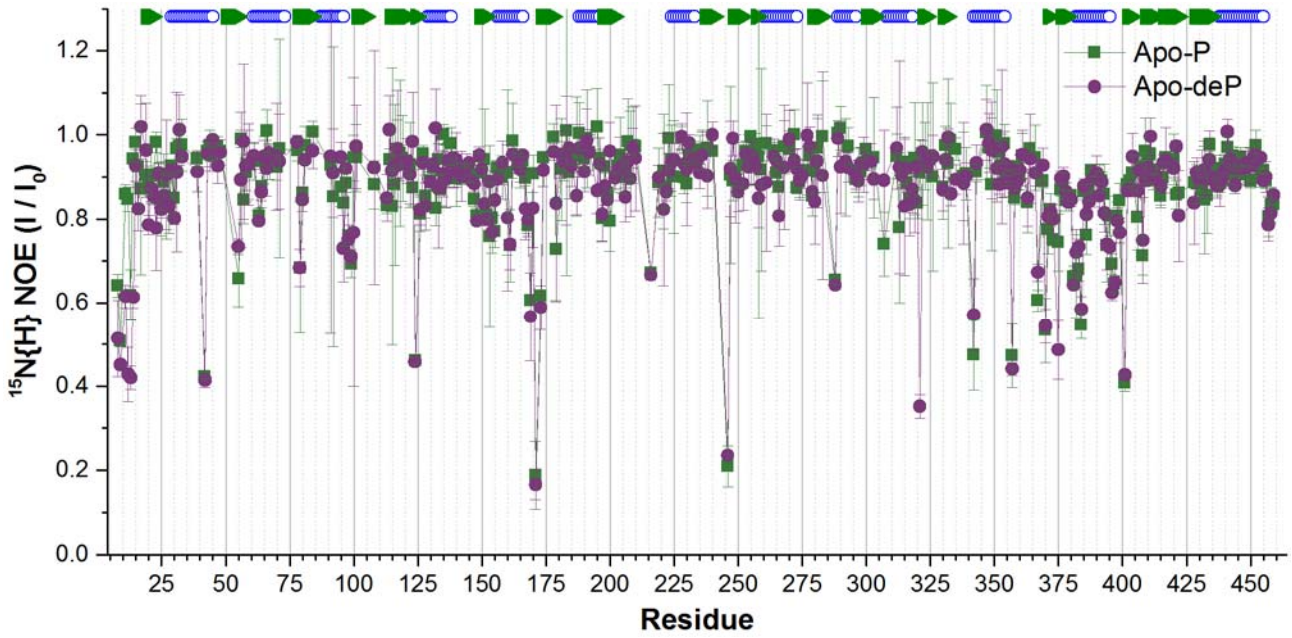

Figure S5. Dependence of $^{15}N\{^1H\}$ heteronuclear, steady-state NOE on phosphorylation status of PMM/PGM. Peak height with ^1H signal saturated is designated I and without saturation as I_0. The measurements were performed in triplicate at 800 MHz and 35 °C. The values plotted are mean ± SD (n= 3) for Apo-P in purple circles and Apo-deP in green squares. The locations of β-strands are marked with green arrows and helices with blue circles.

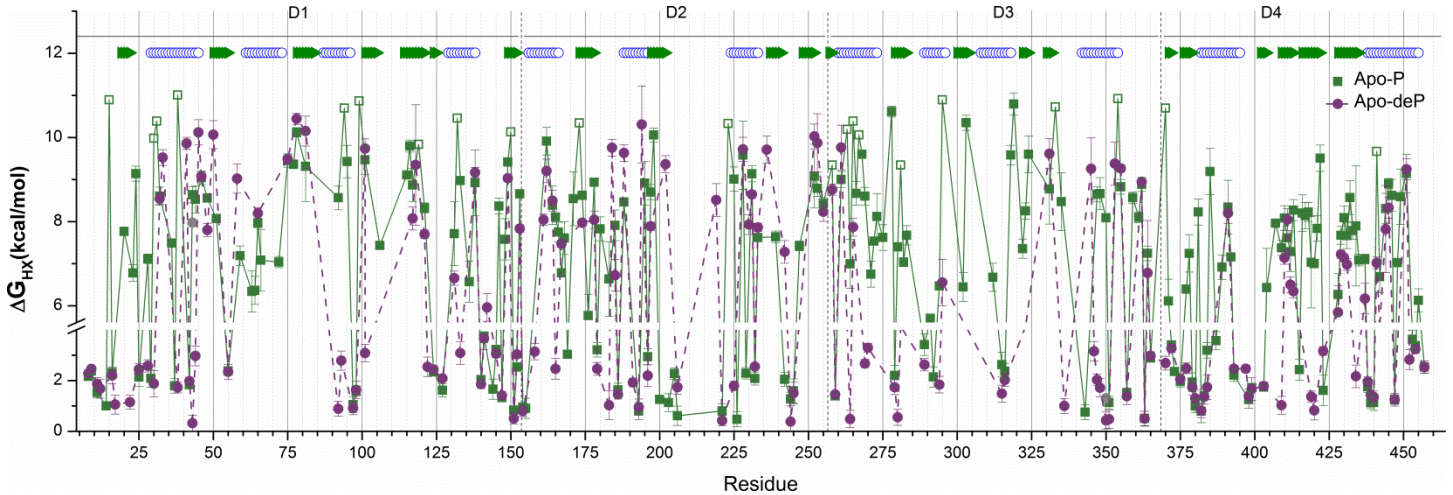

Figure S6. Phosphorylation slows HX and stabilizes domain 3 in particular. ΔG_{HX} values from slow HDX appear above the vertical break, while the small ΔG_{HX} values of rapid HX, measured on the sub-sec scale by CLEANEX-PM NMR (1), appear below the break. Open squares represent lower bounds of the ΔG_{HX} estimates for the especially slowly exchanging amide groups of Apo-P. The locations of strands and helices are marked at the top by triangles and blue circles, respectively.

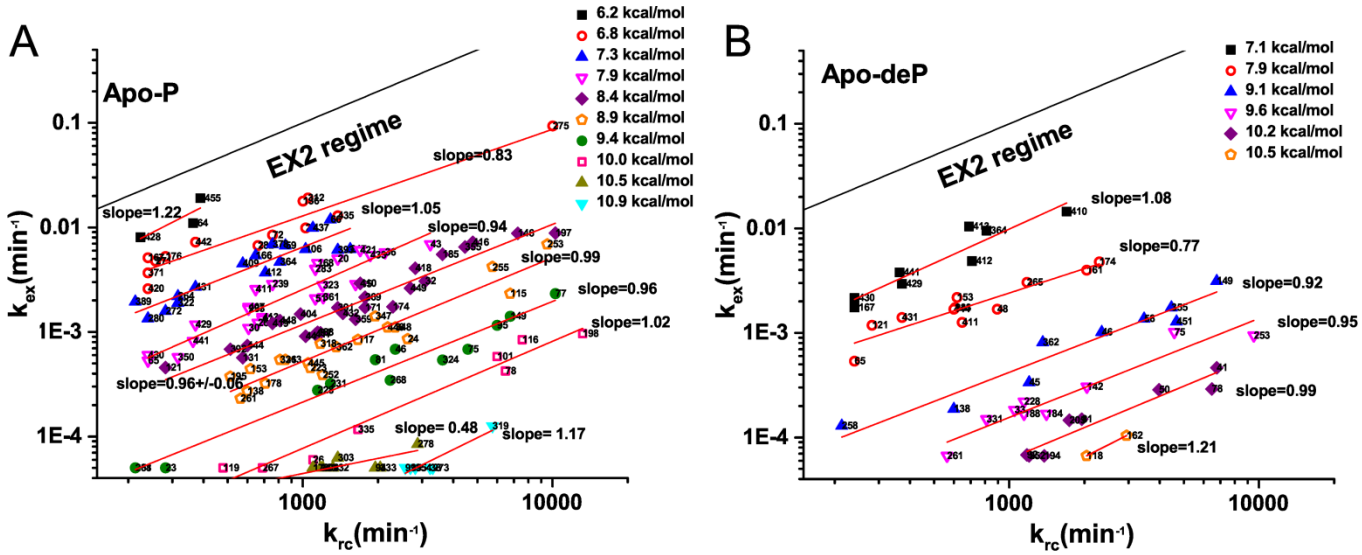

Figure S7. Hydrogen exchange results grouped by $\Delta G_{HDX,apparent}$ suggest the independence of $\Delta G_{HDX,apparent}$ from size of k_{rc}, implying that the EX2 regime prevails for both Apo-P (A) and Apo-deP (B). The reference line depicts the slope of 1.0 typifying the theoretical behavior of the EX2 regime. EX1 has a slope of zero. Residue numbers are listed by each point.

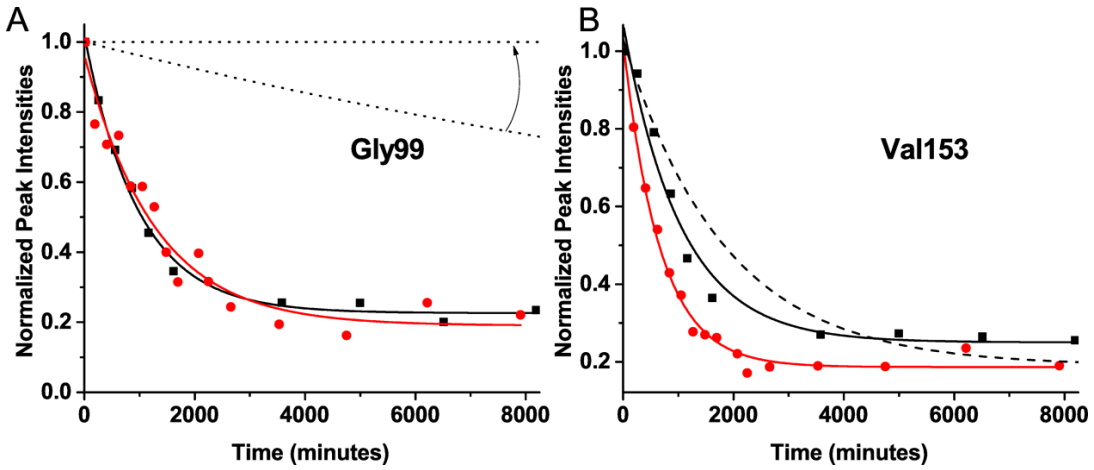

Figure S8. Examples of data fitting of apo-P. Since Apo-P undergoes dephosphorylation, its k_{ex} of HDX is calculated as $k_{ex}=k_{obs}- k_{deP}$. Black squares plot the apparent deuterium exchange curve in D_2O, providing k_{obs}. Red circles plot the decay of the peak in H_2O due to dephosphorylation, providing k_{deP}. Dashed lines mark the computed curve for k_{ex} from which effects of dephosphorylation are removed. (A) In the case of Gly99, the similarity of the two measured decays implies that k_{ex} approaches zero. The upper limit upon its k_{ex} is represented by the lower dashed line. Yet this cannot be experimentally distinguished from $k_{ex} = 0$ represented by the horizontal line, delimiting the other end of the range of potential k_{ex} values. (B) A simple case is illustrated for Val153 where $k_{ex} = k_{obs} – k_{deP}$.

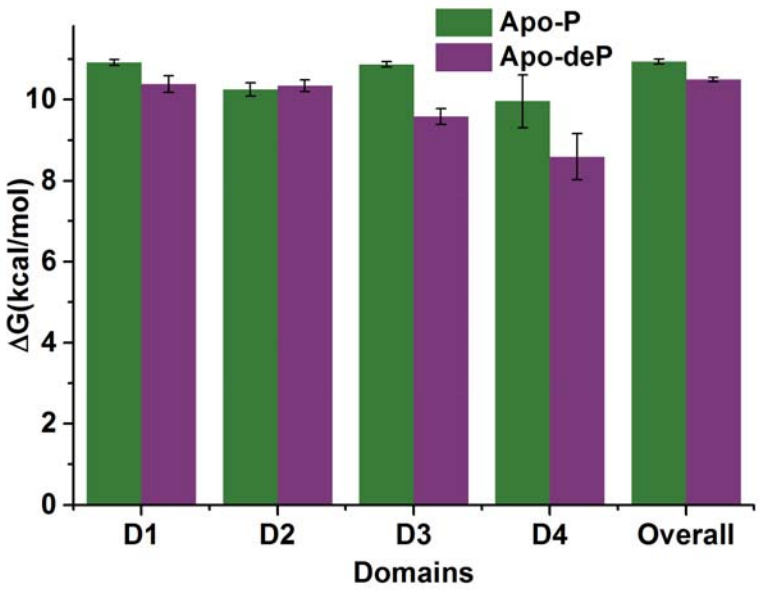

Figure S9. Phosphorylation slows HDX and stabilizes D3 and D4. The three highest ΔG_{HDX} values of each domain, or the enzyme as a whole, suggest the folding stability of that domain and its standard deviation by the method of ref (2) employed. The folding stabilities of Apo-P have been corrected for proline isomerization according to the method (2). The stabilities of Apo-P and its domains 1, 3, and 4 should be regarded as lower limits because the true size of their largest k_{ex} values (used for these ΔG_{fold} estimates) is masked by the rate of dephosphorylation.

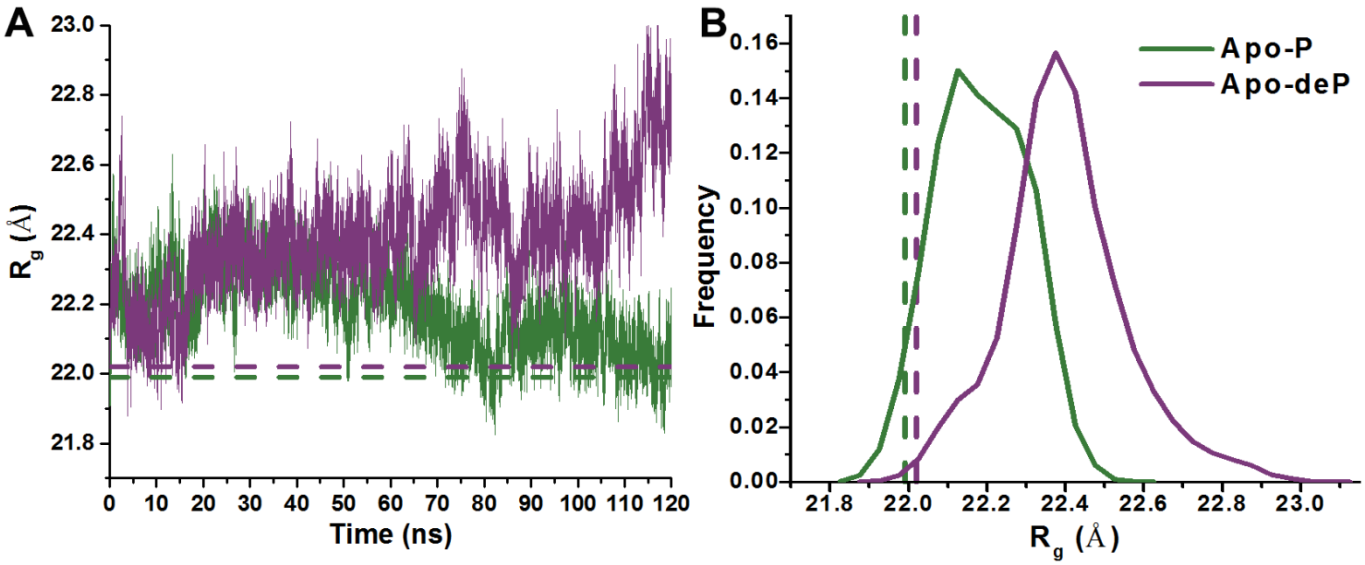

Figure S10. Radii of gyration (R_g) during MD trajectories indicate that the Apo-deP state (purple) is more expanded than Apo-P (green). Dashed lines represent the radii of the crystal structures of Apo-deP and Apo-P (PDB codes 4MRQ and 1K35, respectively). Panel (A) plots the time courses of R_g in the MD trajectories and (B) the histogram of R_g in the trajectories.

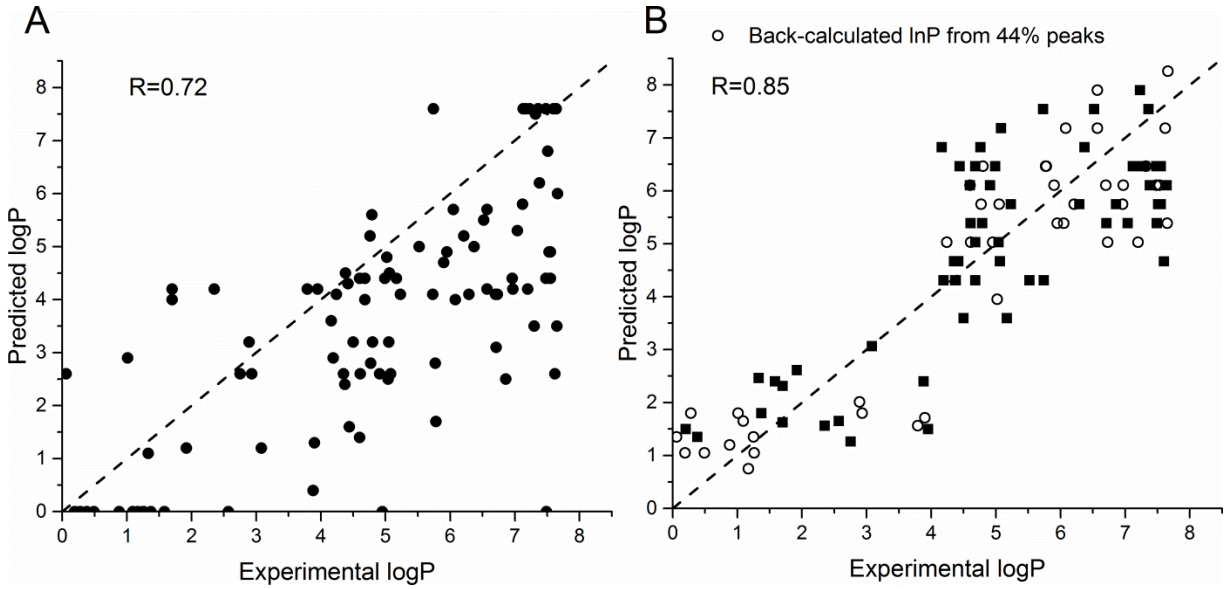

Figure S11. Correlation of experimentally measured HX protection factors *ln(P^{exp})* of staphylococcal nuclease with those simulated from its coordinates using (A) a single set of β_C and β_H coefficients as reported (3) or (B) two sets of coefficients optimized for rapid and slow regimes of HX using 44% of its residues (black squares); see eq. 3. The correlation is effective for the randomly chosen 31% of its residues not used in the optimization (open circles). (The other 25% of residues were not detected). Use of the two sets of coefficients (B) clearly improves the correlation of *ln(P^{sim})* compared with use of a single pair of coefficients (A); see Table S3.

SUPPORTING METHODS

$^{15}N\{^1H\}$ NOE

$^{15}N\{^1H\}$ steady-state NOE relaxation was measured with a Bruker Avance III 800 MHz NMR spectrometer using a pulse sequence with TROSY-enhanced ^1H resolution and sensitivity (4). In order to measure the protein under identical conditions, saturated and unsaturated $^{15}N\{^1H\}$ NOE spectra were collected in an interleaved manner. Each of the triplicate measurements of pairs of spectra of Apo-P was performed on freshly phosphorylated enzyme within 14 h of the phosphorylation. The triplicate measurements of spectra of Apo-deP were performed on freshly dephosphorylated enzyme in 17 h each. All samples were protected from oxidation with 10 mM DTT, Ar, and sealing with Shigemi tube plunger and parafilm.

Correction of HDX decays for lingering solvent

Since the HDX series were initiated by 5-fold dilution with D_2O-based buffer, 20% of solvent was still ^1H_2O. The initial mixture decays as: $A(t) = A_0 \exp(-k_{obs} \times t) + A_\infty$, where the eventual peak size $A_\infty = 0.2 \cdot A_0$ reflects the original H_2O still present at 20%. The ~20 min dead time for sample handling, t_d, delayed acquisition of the first BEST-TROSY spectrum. The exponential decay following the dead time was fitted as:

$$A(t') = A'_0 \exp(-k_{obs} \times t') + A'_\infty \qquad \text{(eq. S1)}$$

where $A'_0 = A(t_d) = A_0 \exp(-k_{obs} \times t_d) + A_\infty$ and A'_∞ required fitting for each decaying peak because:

$$A'_\infty = \frac{A_\infty}{A_0 \exp(-k_{obs} \times t_d) + A_\infty} > 0.2 \times A'_0$$

A'_∞ exceeding 20% of A'_0 is evident in Fig. 2D.

Rate of dephosphorylation and correction of affected rates of HDX

In order to monitor the longevity of the phosphorylated form PMM/PGM and quantify the loss of its phosphorylation as the rate constant k_{deP}, control NMR experiments were set up in H_2O and acquired very similarly to those in D_2O. Decay rates in H_2O solvent were obtained by fitting a single exponential decay rate k_{deP} to the peak heights (Figs. 2D and S2C). Fitting peak heights and volumes gave equivalent results using eq. 2. However, 12 peaks of Apo-P and 10 peaks of Apo-deP underwent small, scattered shifts of the peak centers that introduced modest scatter to the decays; this was rectified using manual picking and volume integration of these peaks. Uncertainties were estimated from spectral noise and fitting errors. Global fitting of the decays of 43 peaks characteristic of Apo-P together with the concurrent increases of the peaks of Apo-deP of the same 43 residues, measured in spectra in H_2O (Fig. S2, C and D), provided the most reliable estimate of k_{deP}.

The rate constants of HDX (k_{ex}) of Apo-P form were corrected for its dephosphorylation by subtracting apparent k_{deP} from the observed rate constant of overall decay after dilution into D_2O: $k_{ex} = k_{obs} - k_{deP}$ (Fig. S8). For 98 Apo-P peaks without overlap with their counterparts of Apo-deP, each peak was corrected by its apparent k_{deP} values fitted independently to the decay of the corresponding peak measured in H_2O spectra. Most of the individually measured decays from dephosphorylation conform to the shared time constant of 19 h for dephosphorylation (Fig.

S2, C and D). However, 14 peaks were subject to an additional faster decay process in H_2O with a time constant of ~4.5 h which we fitted independently to generate pseudo k_{deP} values for use in correcting k_{ex}. Consequently, the decay rates of each individual peak in H_2O spectra were used in correcting the k_{obs} values in D_2O to the k_{ex} of HDX for the 98 amide peaks of Apo-P in the first two categories listed in Table S1. The globally fitted best estimate of k_{deP} was used to correct the k_{ex} of 44 peaks characteristic of Apo-P but overlapped with the corresponding peaks of Apo-deP, which are listed in the third and fourth categories in Table S1.

The k_{ex} rate constants of some well-protected residues appear to be nearly zero (Fig. S8A and S6, open squares). Therefore, upper bounds on k_{ex} were estimated in these most-protected cases. The smallest k_{obs} fitted to HDX spectra was 5.56×10^{-5} min^{-1}, suggesting that the slowest k_{ex} in the enzyme should be less than 5.56×10^{-5} min^{-1}.

In the HDX experiments, 13 residues with overlapped Apo-P and Apo-deP peaks in the TROSY spectra displayed k_{ex} unaffected by phosphorylation. *No correction* for rate of dephosphorylation was needed for these (fifth category of Table S1), as justified in the following section deriving behaviors possible with overlapped peaks.

Fitting of HDX decays of Apo-P peaks where overlapping Apo-deP peaks could develop during the time course

It can be demonstrated that the HDX decays of the overlapped NMR peaks of the phosphorylated and dephosphorylated enzyme forms can be described by this expression encompassing a wide range of scenarios:

$$Pe^{-(k_{ex,P}+k_{deP})t} + Qe^{-k_{ex,deP}t} \qquad \text{(eq. S2)}$$

where $P = \frac{a(k_{ex,P}-k_{ex,deP})}{k_{ex,P}-k_{ex,deP}+k_{deP}}$ and $Q = \frac{(1-a)(k_{ex,P}-k_{ex,deP})+k_{deP}}{k_{ex,P}-k_{ex,deP}+k_{deP}}$,

where *a* is the fraction of the enzyme in the phoshorylated state Apo-P, $k_{ex,P}$ is the rate constant of H(D)X of Apo-P, $k_{ex,deP}$ the rate constant of H(D)X of Apo-deP, and k_{deP} the rate constant for the dephosphorylation. a = 0.9 in the experiments reported herein, minimizing the contribution of the second term. We denote the important comparison $k_{ex,P} - k_{ex,deP}$ as Δk_{ex}. Table S1 summarizes the proper choices of data fitting deduced from use of eq. S2 in different settings.

Eq. S2 indicates that when the Δk_{ex} difference in the HDX rates of the two phosphorylation states is small, then the first term of eq. S2 becomes small. When $\left|\frac{P}{Q}\right| < 0.2$, the term $Pe^{-(k_{ex,P}+k_{deP})t}$ becomes negilible compared to $Qe^{-k_{ex,deP}t}$. Therefore, the kinetic equation for this case of overlapped peaks simplifies to the single exponential decay $Qe^{-k_{ex,deP}t}$ needing no correction because $k_{ex,deP}$ was fitted and $k_{ex,deP} \approx k_{ex,P}$ (Table S1). This situation was recognized at residues where k_{obs} of Apo-P is similar to $k_{ex,deP}$ of Apo-deP.

In cases where phosphorylation causes $k_{ex,P}$ and $k_{ex,deP}$ to differ enough that $|\Delta k_{ex}|$ is enlarged compared to the dephosphorylation rate k_{deP}, the first term of eq. S2 becomes large compared to the second term. When $\left|\frac{Q}{P}\right| < 0.2$, $Qe^{-k_{ex,deP}t}$ becomes negligible compared to $Pe^{-(k_{ex,P}+k_{deP})t}$. In such cases, a single exponential decay with rate constants $k_{ex,P} + k_{deP}$ was observed. This was corrected by subtracting away k_{deP}.

It can be shown (either by derivation or grid search of $k_{ex,P}$ or $k_{ex,deP}$ values) that in the bi-exponential regime (where $0.2 < \left|\frac{P}{Q}\right| < 5$), inappropriate fitting of a single-exponential decay to the bi-exponential decay introduces tolerably little error to resulting estimates of ΔG_{HX}.

Chemical Denaturation

The chemical denaturation of Apo-P and Apo-deP was performed using urea as described (5) but with modifications. 1.3 μM enzyme stock solutions of proteins in 50 mM MOPS, pH 7.4, and 0.1 mM DTT were mixed with this same buffer containing 10 M urea to obtain final urea concentrations ranging up to 8 M. The mixtures were incubated for 12 h. (Longer incubation times give similar denaturation curves.) Trp fluorescence emission was excited at 280 nm and detected at 320 nm using a BioTek Synergy MX plate reader.

Molecular dynamics simulations

The crystal structures of the Apo-P and Apo-deP forms of PMM/PGM (PDB codes 1K35 and 4MRQ, respectively) provided the initial structures. All crystallographic waters were included in the simulations. Hydrogen and missing side chain atoms were added using xleap (6). The Amber ff99SB force field was applied to all residues except the metal binding site (7). The region around the metal-binding site was parameterized as described for the electrostatic calculations. The protonation of the enzyme was set by neutral pH with the pSer108 deprotonated, consistent with the catalytic mechanism (8). The simulations were carried out using GROMACS 4.5.5 (9, 10) on the high performance computing facility at the University of Missouri Bioinformatics Consortium. The enzyme coordinates were solvated in a 10 Å truncated octahedral box containing about 13,000 TIP3P waters and neutralized with Na^+ ions. Moderate Langevin dynamics with a collision frequency of r = 1 ps^{-1} were applied. The cutoff for non-bonded interactions was 10 Å. The SHAKE algorithm was applied (11). After initial minimization, stepwise heating to 10, 50, 100, 150, 200, 250, and 310 K (12) was performed. The system was equilibrated under constant volume for 100 ps and then under constant pressure for another 100 ps. The 60-ns production simulations used periodical boundary condition in an NPT ensemble. The temperature was maintained at 310 K and pressure 1 atm using Berendsen thermostat and Parrinello-Rahman barostat algorithms (13, 14), respectively.

HX protection simulated from MD trajectories

Previous efforts to simulate HX protection, i.e. $\ln\left(P_n^{sim}\right)$, from simulations and structures assumed that the contributions of contacts and hydrogen bonding or $RMSF^{-1}$ to the protection are identical for all residues (15-17). However, as each residue could have a unique environment, the contributions may vary. Therefore, we clustered all residues into two groups, those with more or less protection from measured hydrogen exchange. We optimized independent sets of βc and β_H or $\beta_{1/RMSF}$ for these two clusters of residues, using the same type of optimization of the difference between $\ln\left(P_n^{sim}\right)$ from unrestrained MD simulations and

experimentally measured $\ln(P_n^{exp})$ as described by Kieseritzky et al (17), i.e. minimizing this RMS deviation:

$$\Delta lnP = \sqrt{\frac{1}{N}\sum_{n=1}^{N}\left(\ln(P_n^{sim}) - \ln(P_n^{exp})\right)^2} \quad \text{(eq. S3)}$$

Two alternative sets of βc and β_H for quickly or slowly exchanging sites turned out to better simulate the protections and minimize the overall ΔlnP than did a single set of coefficients, for a set of well-characterized model proteins and their structures (Table S3) and for the PMM/PGM enzyme and its MD trajectories (Table S4).

In the tallying of structural interactions for the optimization process, contacts N_n^c between two residues were defined when the distances between amide nitrogen and heavy atoms are closer than 6.5 Å (16). Hydrogen bonds N_n^h were considered as formed for H-O distances shorter than 2.4 Å and N-H-O angles greater than 140 °. The errors were calculated as the standard deviations of the time-averaged protection factor elements (PFEs, e.g. N_n^c and N_n^h) counted from the trajectories. Since well-protected amide groups should be observed by NMR-detected HDX, $\beta_c^{\text{less prot}}$ and $\beta_H^{\text{less prot}}$ or $\beta_{1/RMSF}^{\text{less prot}}$ were used to calculate $\ln(P_n^{sim})$ of residues that were not detected by HDX or CLEANEX-PM in plotting Fig. 6C. The good correlations between $\ln(P_n^{sim})$ and $\ln(P_n^{exp})$ (Tables S3 and S4, Fig. S11 and 6B) suggest that $\ln(P_n^{sim})$ could be used as a proxy for $\ln(P_n^{exp})$ for the numerous amide groups of PMM/PGM in the unmeasured time regime of HX slower than 12 s and faster than 20 min; compare Fig. 3A and 6C.

Table S1. Behaviors of amide TROSY NMR peaks of Apo-P monitored by HDX and the appropriate data fitting method implemented.

Category	Count	Data Fitting
Total peaks of Apo-P tracked by HDX	155 (68%) *	
Residues with well-resolved peaks for Apo-P and Apo-deP	87 (38.2%)	Single exponential $k_{obs} = k_{ex,P} + k_{deP}$ †
Only Apo-P peaks present as Apo-deP peaks were missing	11 (4.8%)	Single exponential $k_{obs} = k_{ex,P} + k_{deP}$ †
Overlapped peaks	57 (36.7%)	
Apo-deP peak decayed too quickly to be seen by HDX-NMR. ‡	31 (13.6%)	Single exponential §‡ $k_{obs} = k_{ex,P} + k_{deP}$
Phosphorylation changes k_{ex} significantly: $\Delta k_{ex} < -3.6k_{deP}$ or $\Delta k_{ex} > 12.5k_{deP}$, $\left\|\frac{Q}{P}\right\| < \mathbf{0.2}$ ¶	13 (5.7%)	Single exponential $k_{obs} = k_{ex,P} + k_{deP}$ §
Little effect of phosphorylation: $\|\Delta k_{ex}\| < 0.22k_{deP}$, $\left\|\frac{P}{Q}\right\| < \mathbf{0.2}$	13 (5.7%)	Single exponential $k_{obs} = k_{ex,P} = k_{ex,deP}$
$\mathbf{0.2} < \left\|\frac{P}{Q}\right\| < \mathbf{5}$	0 (0%)	Bi-exponential See eq. S2

* % of the total amide peaks monitored are given in parentheses

† Apparent k_{deP} values for each of these individual residues (individually fitted to the decay of each NMR peak in H_2O) were used to accommodate the anomalously fast decay of 14 of these 98 peaks (a group with time constant of 4.5 ± 0.1 h and "k_{deP}" of ~3.7 x 10^{-3} min^{-1}).

‡ $k_{ex,deP}$ was rapid, apparently > 0.05 min^{-1}

§ The globally fitted value of k_{deP} was used to correct the k_{ex} values of Apo-P.

¶ $\Delta k_{ex} = k_{ex,P} - k_{ex,deP}$. P and Q are defined by eq. S2.

Table S2. NMR identification of residues with HX altered by Ser108 phosphorylation, clarifying behaviors within peptides obscured in HDX-MS results

	Peptide residues*	Stabilized by phosphorylation	Destabilized by phosphorylation	Little change†
Partly overlapping active site	92-117‡	92, 95,106,115,116	Not detected	93,97,98, 101,117
	205-239	223,239	206,219,230,236	221,225,228,229, 231-233
	240-266	244,247,263-266	242	245,252,253,255, 258,259,261
	267-293	268,269,271-273, 275,278,280-282,291	Not detected	270,279,289,292
	323-346	323,324,333,335,336	343, 345	331, 346
Far from active site				
	28-44	28,30,36,38,44	33,37,41	29,32,42,43
	45-52	Not detected	45,50	46,48
	53-78	59,63,64,66,72,77	58	55,65,75,78
	169-191	171,173,174,176, 178,180,183,185	184, 188	169,179,186,191
	192-204	195,197,198,	194,202,203	193,196,200
	378-406	378,381,384, 385,389, 392,404	Not detected	379,380,382,383,387, 391,393,397,398,399,403
	407-429	407,409,410,413, 416-422	Not detected	411,412,415,428,429
	442-463	442,446,448,449,455	Not detected	444,445,447, 451-454,457

* Peptides were generated by pepsinolysis. Percentage increase in deuteration of peptide as a whole was measured by mass spectrometry (18).

† Insufficient evidence of a difference greater than 1 kcal/mol

‡ The phosphopeptide evaded detection by HDX-MS.

Table S3. Comparison of one and two sets of coefficients in modeling HX protection factors from surrounding contacts and hydrogen bonds for well-characterized proteins

Protein	One pair of coefficients				Two pairs of coefficients					
					less protected residues		more protected residues			
	β_C*	β_H†	ΔlnP‡	Pearson's correlation coefficient	β_C*	β_H†	β_C*	β_H†	ΔlnP ‡	Pearson's correlation coefficient
Ubiquitin§	0.35¶	2.00¶	3.73	0.75	0.48	1.06	0.75	1.39	1.72	0.88
	0.58‖	2.30‖	2.33	0.75						
Staphylo-coccal nuclease**	0.35¶	2.00¶	2.07	0.64	0.13	0.79	0.35	1.26	1.19	0.85
	0.27‖	1.80‖	1.71	0.64						
bacterial cytochrome c ††	0.35¶	2.00¶	3.04	0.58	0.51	0.36	0.65	0.28	1.57	0.77
	0.60§§	1.59§§	1.86§§	0.62§§						

* Coefficient for the number of contacts surrounding each residue (15)

† Coefficient for the number of hydrogen bonds to each backbone amide group (15)

‡ Difference in natural logarithm of simulated and experimental protection factor P (15); smaller indicates better agreement.

¶ Optimized in ref (16)

‖ Parameters optimized for measured HX protection factors following the method of ref (17).

§§ From ref (17)

§ Protection factors were calculated from rates of HX of ref (19). PDB: 1UBI

** HX protection factors from ref (3). PDB: 1SNO. Hydrogen atoms were added to the coordinates using Sybyl 7.3.

†† HX protection factors are digitized from Fig. 2 of ref (20), PDB: 1K3G (first conformer).

Table S4. Comparison of HX protection factors measured and simulated from MD trajectories, ΔlnP, of PMM/PGM, using one or two pairs of coefficients for protection factor elements (PFE)

Phosphorylation state	PFE1, no. of contacts	PFE2	less protected residues		more protected residues		ΔlnP	Pearson's correlation coefficient
			β_c	β_2	β_c	β_2		
Apo-P	N_n^c	N_n^h	0.35	2.0*	0.35	2.0*	6.7	0.34
Apo-deP							5.5	0.36
Apo-P	N_n^c	N_n^h	0.22	0.68	0.80	2.50	3.2	0.82
Apo-deP							2.6	0.89
Apo-P	N_n^c	$RMSF^{-1}$	0.22	0.28†	0.56	3.94†	3.1	0.83
Apo-deP							2.7	0.88

* The single pair of coefficients optimized by ref (16) was applied and is listed twice.

† These two pairs of coefficients were used to generate Fig. 6, B and C.

Supporting References

1. Hwang, T. L., P. C. van Zijl, and S. Mori. 1998. Accurate quantitation of water-amide proton exchange rates using the phase-modulated CLEAN chemical EXchange (CLEANEX-PM) approach with a Fast-HSQC (FHSQC) detection scheme. Journal of Biomolecular NMR 11:221-226.
2. Huyghues-Despointes, B. M., J. M. Scholtz, and C. N. Pace. 1999. Protein conformational stabilities can be determined from hydrogen exchange rates. Nat. Struct. Biol. 6:910-912.
3. Skinner, J. J., W. K. Lim, S. Bedard, B. E. Black, and S. W. Englander. 2012. Protein hydrogen exchange: testing current models. Protein Sci. 21:987-995.
4. Zhu, G., Y. Xia, L. K. Nicholson, and K. H. Sze. 2000. Protein Dynamics Measurements by TROSY-Based NMR Experiments. J. Magn. Reson. 143:423-426.
5. Fulcher, Y. G., and S. R. Van Doren. 2011. Remote exosites of the catalytic domain of matrix metalloproteinase-12 enhance elastin degradation. Biochemistry 50:9488-9499.
6. Case, D. A., T. A. Darden, T. E. Cheatham, C. L. Simmerling, J. Wang, R. E. Duke, R. Luo, R. C. Walker, W. Zhang, K. M. Merz, B. Roberts, S. Hayik, A. Roitberg, G. Seabra, J. Swails, A. W. Goetz, I. Kolossváry, K. F. Wong, F. Paesani, J. Vanicek, R. M. Wolf, J. Liu, X. Wu, S. R. Brozell, T. Steinbrecher, H. Gohlke, Q. Cai, X. Ye, M. J. Hsieh, G. Cui, D. R. Roe, D. H. Mathews, M. G. Seetin, R. Salomon-Ferrer, C. Sagui, V. Babin, T. Luchko, S. Gusarov, A. Kovalenko, and P. A. Kollman. 2012. AMBER 12. University of California, San Francisco.
7. Hornak, V., R. Abel, A. Okur, B. Strockbine, A. Roitberg, and C. Simmerling. 2006. Comparison of multiple Amber force fields and development of improved protein backbone parameters. Proteins: Structure, Function, and Bioinformatics 65:712-725.

8. Naught, L. E., and P. A. Tipton. 2001. Kinetic Mechanism and pH Dependence of the Kinetic Parameters of *Pseudomonas aeruginosa* Phosphomannomutase/Phosphoglucomutase. Archives of Biochemistry and Biophysics 396:111-118.
9. Berendsen, H. J. C., D. van der Spoel, and R. van Drunen. 1995. GROMACS: A message-passing parallel molecular dynamics implementation. Comput. Phys. Commun. 91:43-56.
10. Lindahl, E., B. Hess, and D. van der Spoel. 2001. GROMACS 3.0: a package for molecular simulation and trajectory analysis. J Mol Model 7:306-317.
11. Ryckaert, J.-P., G. Ciccotti, and H. J. C. Berendsen. 1977. Numerical integration of the cartesian equations of motion of a system with constraints: molecular dynamics of n-alkanes. Journal of Computational Physics 23:327-341.
12. Xu, J., G. Yin, and W. Du. 2011. Distal mutation modulates the heme sliding in mouse neuroglobin investigated by molecular dynamics simulation. Proteins 79:191-202.
13. Berendsen, H. J. C., J. P. M. Postma, W. F. van Gunsteren, A. DiNola, and J. R. Haak. 1984. Molecular dynamics with coupling to an external bath. J. Chem. Phys. 81:3684-3690.
14. Parrinello, M., and A. Rahman. 1981. Polymorphic transitions in single crystals: A new molecular dynamics method. J. Appl. Phys. 52:7182-7190.
15. Vendruscolo, M., E. Paci, C. M. Dobson, and M. Karplus. 2003. Rare fluctuations of native proteins sampled by equilibrium hydrogen exchange. J. Am. Chem. Soc. 125:15686-15687.
16. Best, R. B., and M. Vendruscolo. 2006. Structural Interpretation of Hydrogen Exchange Protection Factors in Proteins: Characterization of the Native State Fluctuations of CI2. Structure 14:97-106.
17. Kieseritzky, G., G. Morra, and E.-W. Knapp. 2006. Stability and fluctuations of amide hydrogen bonds in a bacterial cytochrome c: a molecular dynamics study. J. Biol. Inorg. Chem. 11:26-40.
18. Lee, Y., M. T. Villar, A. Artigues, and L. J. Beamer. 2014. Promotion of Enzyme Flexibility by Dephosphorylation and Coupling to the Catalytic Mechanism of a Phosphohexomutase. J. Biol. Chem. 289:4674-4682.
19. Bougault, C., L. Feng, J. Glushka, E. Kupče, and J. H. Prestegard. 2004. Quantitation of rapid proton-deuteron amide exchange using hadamard spectroscopy. J. Biomol. NMR 28:385-390.
20. Bartalesi, I., A. Rosato, and W. Zhang. 2003. Hydrogen exchange in a bacterial cytochrome c: a fingerprint of the cytochrome c fold. Biochemistry 42:10923-10930.